



Gold nanoparticles decorated Ag(Cl,Br) micro-necklaces for efficient and stable SERS detection and visible-light photocatalytic degradation of Sudan I

Qi Cao ^{a,b}, Xin Liu ^b, Kaiping Yuan ^c, Jun Yu ^b, Qinghe Liu ^b, Jean-Jacques Delaunay ^b, Renchao Che ^{a,*}

^a Laboratory of Advanced Materials, Department of Materials Science, Collaborative Innovation Center of Chemistry for Energy Materials, Fudan University, 2205 Songhu Road, Shanghai, 200438, People's Republic of China

^b School of Engineering, The University of Tokyo, Hongo 7-3-1, Bunkyo-ku, Tokyo, 113-8656, Japan

^c State Key Laboratory of ASIC and System, School of Microelectronics, Fudan University, 220 Handan Road, Shanghai, 200433, People's Republic of China



ARTICLE INFO

Article history:

Received 16 May 2016

Received in revised form 7 July 2016

Accepted 1 September 2016

Available online 1 September 2016

Keywords:

silver halides

plasmonic photocatalysis

food contamination

Sudan dyes

Surface-enhanced Raman spectroscopy

ABSTRACT

In this paper, we report an air-exposed and room-temperature immersion reaction for synthesis of novel Au nanoparticles decorated Ag(Cl,Br) [Ag(Cl,Br)–Au] micro-necklaces from the AgBr template for efficient and stable photocatalytic degradation and SERS detection of food contaminant Sudan I (SDI) molecules. Amazingly, as the photocatalyst, the partial substitution of bromine atoms by chlorine in crystalline lattices and decoration of Au nanoparticles on the surface have synergistically ensured these Ag(Cl,Br)–Au micro-necklaces of enhanced degradation efficiency of SDI from 65.1% achieved by AgBr to 100% after 18 min of visible light irradiation, along with significantly promoted efficiency maintenance after 12 cycles of the photocatalytic reaction. Meanwhile, due to the designed decoration of Au nanoparticles on surfaces of semiconducting micro-necklaces, these Ag(Cl,Br)–Au micro-necklaces also exhibited the ability to offer sensitive SERS signals for trace detection of SDI molecules with the limit of detection as low as 10^{-10} M being achieved. Hence, in consideration of the novel structures, facile preparation as well as attractive applications in both SERS detection and photocatalytic degradation of SDI dye of these Ag(Cl,Br)–Au micro-necklaces, it is believable that such bifunctional substrate materials hold great potential for various environmental and health-related applications.

© 2016 Elsevier B.V. All rights reserved.

1. Introduction

The food contamination scandals occurred worldwide in the past decade have forced people to put intense focus on Sudan I (SDI, 1-phenylazo-2-naphthol) dye as a potential carcinogen which may cause DNA damage and cancer [1–3]. Researchers therefore have made a great effort to develop efficient approaches for trace detection of SDI. Till now, a number of analytical techniques, including the optical sensing (fluorescence [4] and surface plasmon resonance [5,6]), high-performance liquid chromatography, [7–10] enzyme-linked immunosorbent assay, [11–15] electrochemical methods [16–20] and so on, have been developed for molecular detection of SDI, among which the surface-enhanced Raman scattering (SERS) spectroscopy [21–30] might be the most promising

one. As an extremely sensitive and surface-selective technique, SERS spectra can be tailored on substrate materials to provide rapid detections of organics down to single-molecule level [31–33]. A booming trend in the research of trace determination of food contamination and other organic pollutants by SERS spectroscopy is to introduce the process of photocatalysis simultaneously into the same substrate systems to achieve in-situ degradation of such organics as well. The combination and integration of SERS substrates with photocatalytic materials have so far triggered several promising applications like photocatalytic degradation induced self-cleaning SERS platforms [34–37], or inversely, the in-situ SERS monitoring and even quantitative probing of surface plasmon-promoted catalytic reactions [38–45]. Nevertheless, in spite of few reports on Sudan III and IV degradation [46–48], neither the photocatalytic degradation of SDI molecules itself, nor the simultaneous SERS detection and photocatalytic degradation for SDI received adequate research [24,49].

* Corresponding author.

E-mail address: rcche@fudan.edu.cn (R. Che).

Silver halide compounds, for example the silver bromide (AgBr) and silver chloride (AgCl), are important light-sensitive materials and plasmonic photocatalysts. However, their optical instability as well as feasibility of decomposition have inhibited them to be high-performance single-component photocatalysts. The grains of silver halide materials are photosensitive due to their point ionic defects and electron traps by silver ions of high mobility [50,51]. Hence for application, these silver halides are usually coupled with noble metals [52–56] and other semiconductor materials [57–59] to promote charge separation by metallic electron sinks or semiconductor p - n junctions, and thus inhibit the combination between photoelectrons and either silver ions or photoholes at interfaces, so that they can finally become plasmonic photocatalysts with considerable structural stability and high efficiency under visible light irradiation. The properties of $\text{Ag}(\text{Cl},\text{Br})$ are similar to other silver halides like AgBr and AgCl while it has been seldom studied before [60]. Just like the case of AgBr and AgCl , only if the photoelectrons are prevented effectively from combining with silver ions and photoholes, such $\text{Ag}(\text{Cl},\text{Br})$ materials can be novel and stable photocatalysts. So far, only Huang et al. have once prepared the $\text{Ag}@\text{Ag}(\text{Cl},\text{Br})$ powder successfully for visible-light-driven plasmonic photocatalyst [60].

Here in this work, we obtained gold nanoparticles decorated $\text{Ag}(\text{Cl},\text{Br})$ [$\text{Ag}(\text{Cl},\text{Br})-\text{Au}$] micro-necklaces for the first time via an air-exposed and room-temperature immersion reaction accompanied with a mild annealing process from AgBr micro-necklaces facilely grown on pristine silver foils. As a result, these $\text{Ag}(\text{Cl},\text{Br})-\text{Au}$ micro-necklaces have demonstrated stable performance for both photocatalytic degradation and sensitive SERS detection of SDI molecules. Specifically on the one hand, as novel photocatalyst, the partial substitution of bromine by chlorine element and decoration of gold nanoparticles on the surface have synergistically endowed the $\text{Ag}(\text{Cl},\text{Br})-\text{Au}$ micro-necklaces with enhanced degradation efficiency of SDI from 65.1% achieved by AgBr to nearly 100% after 18 min of visible light irradiation. On the other hand, the introduction of gold nanoparticles also enabled the composite micro-necklaces to provide appreciable SERS sensitivity owing to which the limit of detection (LOD) for SDI of as low as 10^{-10} M was finally achieved. Overall, it is believed that the $\text{Ag}(\text{Cl},\text{Br})-\text{Au}$ micro-necklaces presented in this work, with their novel structures, facile preparation as well as attractive applications as bifunctional SERS and photocatalytic substrates toward SDI dye, suggest many opportunities of developing novel multifunctional devices for environmental and health monitoring and management.

2. Experimental section

2.1. Materials and chemicals

Silver foils (Ag, 3N, 0.1 mm thick), polyvinylpyrrolidone (PVP, K-30), iron(III) nitrate nonahydrate ($\text{Fe}(\text{NO}_3)_3 \cdot 9\text{H}_2\text{O}$, AR), potassium bromide (KBr, SP), chloroauric acid tetrahydrate ($\text{HAuCl}_4 \cdot 4\text{H}_2\text{O}$, AR), sodium hydroxide (NaOH, AR), nitric acid (HNO_3 , AR), Sudan I (SDI, BS), absolute ethanol (GR) and acetone (AR) were all purchased from Sinopharm Chemical Reagent Company. All chemicals were used just as received without further purification, and for all experiments, deionized water (DI water, Millipore) with the resistivity greater than $18.0\text{ M}\Omega\text{-cm}$ was used.

2.2. Preparation of the $\text{Ag}(\text{Cl},\text{Br})-\text{Au}$ micro-necklaces

As-purchased silver foils were first cut into pieces ($3 \times 0.5\text{ cm}^2$) and cleaned by dilute nitric acid solution and acetone, respectively. Briefly, a piece of Ag foil was first immersed into the mixture aqueous solution (50 mL) of $\text{Fe}(\text{NO}_3)_3 \cdot 9\text{H}_2\text{O}$ (0.5 M), KBr (0.5 M) and PVP (0.15 M) in air at room temperature for about 8 h to form AgBr

micro-necklaces on the surface according to a literature report [61]. Afterward, the piece of foil was taken out of the mixture solution carefully and rinsed with ethanol and DI water thoroughly. Next, the foil was once again immersed into the aqueous solution containing 0.01 M HAuCl_4 (with the pH value tuned to 7.0 by addition of 0.2 M NaOH solution drop by drop) and maintained for about 3 h. After the foil was again taken out and rinsed by DI water thoroughly, it was dried in air and annealed in air at 300°C for 2 h (with the heating rate set at $5^\circ\text{C}/\text{min}$). The whole process finished when the finally obtained brown gray foil cooled down naturally in air.

2.3. Characterization

Scanning electron microscope (SEM) images and energy dispersive X-ray spectra (EDS) were recorded using a field-emission SEM (FE-SEM, S4800, Hitachi, Japan) equipped with an energy dispersive spectrometer (XFlash 5030, Bruker, Germany). High-resolution transmission electron microscopy (HRTEM) analysis was conducted on a field-emission TEM (FE-TEM, JEOL JEM-2100F, Japan) equipped with a post-column Gatan imaging filter system (GIF, Tridium 863, United States) working at 200 kV of the acceleration voltage. The TEM samples were prepared by ultramicrotome cutting of the fragments of as-synthesized $\text{Ag}(\text{Cl},\text{Br})-\text{Au}$ micro-necklaces obtained by continuous sonification. X-ray diffraction (XRD) measurement was carried out on a powder X-ray diffractometer (D8 Advance, Bruker, Germany) working with $\text{Cu}-\text{K}\alpha$ radiation (1.5406 \AA) at 40 mA and 40 kV. The UV-vis absorbance spectra of SDI solutions and UV-vis-NIR diffuse reflectance spectra (DRS) of the samples were obtained on a Shimadzu UV-3600 (Japan) and a JASCO V-670 (Japan) UV-vis-NIR spectrophotometer, respectively. The Raman and SERS spectra were collected on a laser confocal Raman micro-spectrometer (*inVia* reflex, Renishaw, UK) equipped with an integrated optical microscope (DM-2500, Leica, Germany).

2.4. Details for SERS measurements

Dilute SDI solutions in mixed solvent of ethanol and water (volume ratio = 1:1) were first prepared at different concentrations. A piece of as-obtained sample foil was immersed into the solution at room temperature and kept for 12 h in the dark so that the SDI molecules could fully absorbed onto the surfaces of the $\text{Ag}(\text{Cl},\text{Br})-\text{Au}$ micro-necklaces. The piece of foil was afterward taken out and dried by an infrared lamp for final measurement. Particularly in all measurements, the excitation source of a 632.8 nm He-Ne laser, grating of 1800 1/mm, laser power of 1.7 mW (10% \times 17 mW), exposure time of 10.0 s, accumulation of five times and objective lens of $50 \times /0.50$ were applied. During the recyclability test, the used $\text{Ag}(\text{Cl},\text{Br})-\text{Au}$ foil was recycled and rinsed by absolute ethanol and DI water thoroughly before entering each new cycle. The intensities of selected bands in the SERS spectrum recorded in the first cycle was regarded as the reference (100%).

2.5. Details for photocatalytic measurements

The photocatalytic degradation reaction of SDI was carried out in a quartz cuvette ($1 \times 1 \times 4\text{ cm}^3$, Jingke Optical Instrument, Yixing). Typically, a piece of AgBr or $\text{Ag}(\text{Cl},\text{Br})-\text{Au}$ foil was vertically put into fresh solutions of SDI (3 mL, 10^{-6} M with 1:1 vol ratio of ethanol and water as the solvent) within the quartz cuvette. The cuvette was afterward irradiated by a Xe lamp ($\lambda \geq 420\text{ nm}$, 300 W, Labsolar-IIIAAG, Perfect-Light Company, Beijing) at room temperature. Meanwhile, the UV-vis absorbance spectra of the reaction solutions were quickly recorded at two minutes interval. Just similar to the SERS measurement, the used foils were recycled and

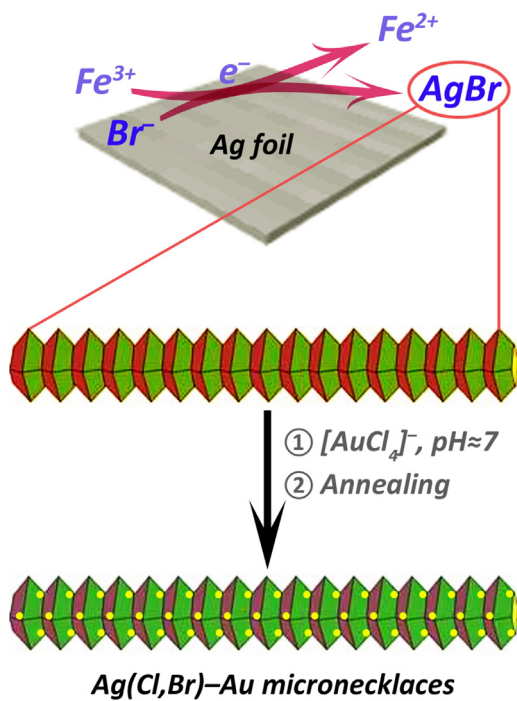


Fig. 1. Schematics of the synthetic process for Ag(Cl,Br)-Au micro-necklaces from pristine silver foils.

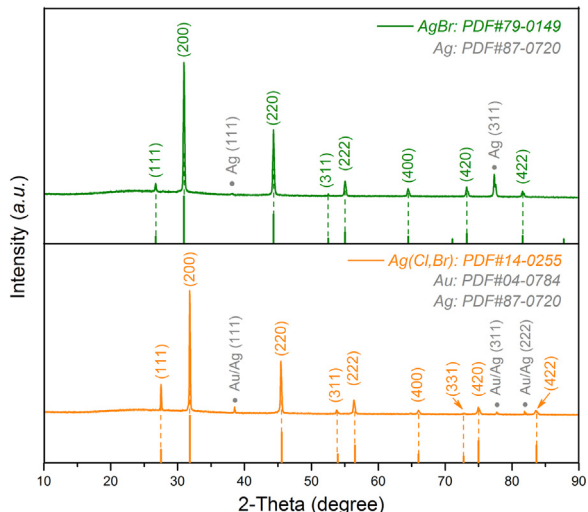


Fig. 2. Representative XRD patterns of the obtained AgBr (green curve) as well as Ag(Cl,Br)-Au (orange curve) micro-necklaces grown on silver foils. (For interpretation of the references to colour in this figure legend, the reader is referred to the web version of this article.)

rinsed thoroughly by ethanol and DI water before entering each new cycle.

3. Results and discussion

The Ag(Cl,Br)-Au micro-necklaces were prepared via a room-temperature air-exposed immersion reaction along with appropriate annealing process. Fig. 1 gives a schematic illustration of the synthetic process for these Ag(Cl,Br)-Au micro-necklaces. First, AgBr micro-necklaces were obtained on pristine Ag foils. The green curves in Figs. 2 and 3 show the representative XRD pattern and Raman spectrum of the AgBr micro-necklaces where all characteristic diffraction peaks and the Raman band located at about

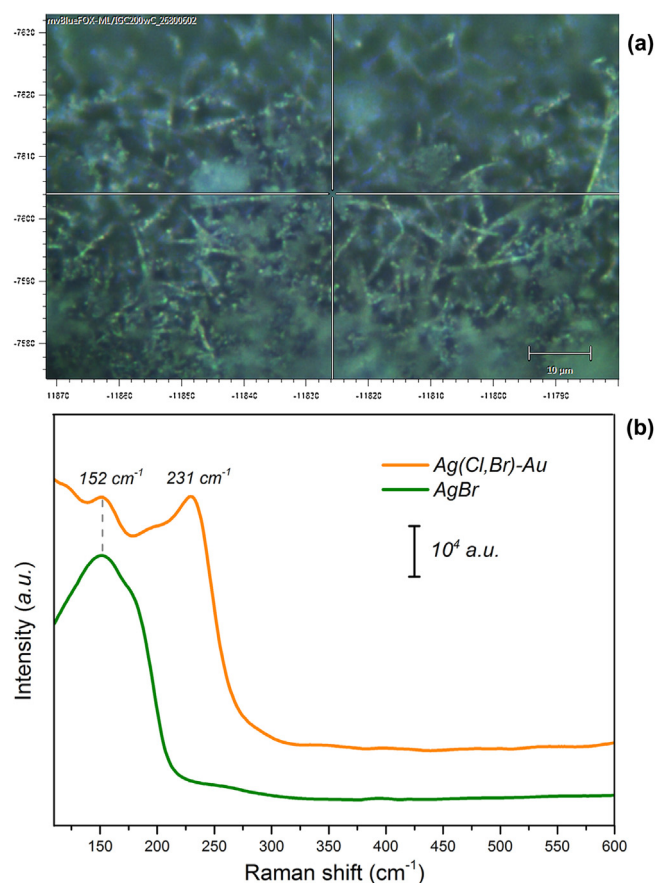


Fig. 3. Raman micro-spectroscopic characterization results: (a) Representative bright-field (BF) optical micrograph of the obtained Ag(Cl,Br)-Au micro-necklaces and (b) room-temperature Raman spectra of the Ag(Cl,Br)-Au and AgBr micro-necklaces grown on silver foils. The orange curve in panel (b) was recorded correspondingly from the central area in panel (a). (For interpretation of the references to colour in this figure legend, the reader is referred to the web version of this article.)

152 cm⁻¹ can be assigned to the pure cubic $Fm(-3)m$ phase of AgBr (PDF#79-0149) and the stretching mode of Ag–Br bond respectively [62,63], demonstrating the formation of a AgBr layer on silver foils clearly. Afterward, by immersing the obtained AgBr micro-necklaces in the aqueous solution of HAuCl₄, bromine atoms were partially substituted by chlorine atoms. At the same time, gold clusters deposited on the surfaces of micro-necklaces and transformed into gold nanoparticles finally after the aggregation accompanied by Ostwald ripening process had happened during annealing [45]. The orange curve in Fig. 2 of the XRD pattern reveals the unique cubic $Fm(-3)m$ phase of Ag(Cl,Br) (PDF#14-0255) with all characteristic peaks matching quite well. Besides, three small peaks at around 38.2, 77.6 and 81.8 ° of 2θ which can be indexed to the (111), (311) and (222) crystal planes of cubic phase of gold (PDF#04-0784) or silver (PDF#87-0720) suggest the possibility for the existence of small Au nanoparticles. In the room-temperature Raman spectrum (Fig. 3), for the case of the finally obtained Ag(Cl,Br)-Au micro-necklaces, besides the scattering band at 152 cm⁻¹, the band at about 231 cm⁻¹ which derived from the stretching mode of Ag–Cl bond [64,65] can be obviously observed as well, confirming the formation of the Ag(Cl,Br) phase. Moreover, the HRTEM analysis of different parts of the Ag(Cl,Br)-Au micro-necklaces (i.e. Ag(Cl,Br) microcrystals and gold nanoparticles) are presented in Fig. S1–S2 of the Supplementary data, by which the presence and phase purity of Ag(Cl,Br) micro-necklaces and gold nanoparticles could be further demonstrated.

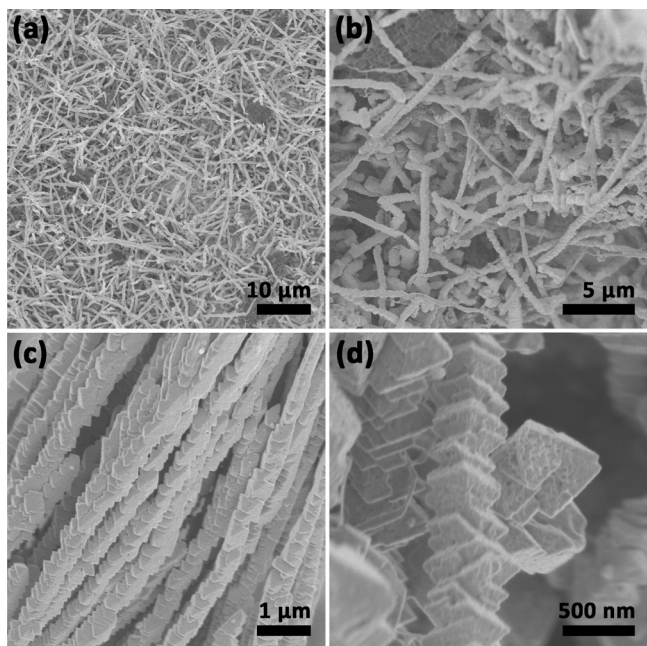


Fig. 4. Representative SEM images recorded at different magnifications of the synthesized AgBr micro-necklaces. The image in panel (c) was taken from an area where the AgBr micro-necklaces occasionally aligned with each other.

Figs. 4,5 and **Fig. 3a** exhibit the SEM images of the AgBr and Ag(Cl,Br)-Au micro-necklaces, and the BF optical micrograph of the Ag(Cl,Br)-Au micro-necklaces, respectively. It is obvious that both AgBr and Ag(Cl,Br)-Au have distinct chain-like morphologies. Nevertheless, the composing units of AgBr appear more like polyhedrons (**Fig. 4c-d**) while the composing units of Ag(Cl,Br)-Au seem to be not so sharp and angular any more (**Fig. 5b-c**), indicating that the simultaneously occurred processes of Cl substitution and Au deposition in aqueous solutions might have led to the surface etching of the original AgBr chain-like structures as well so that the finally obtained Ag(Cl,Br)-Au micro-structures turned out to be more like connected beads, which are both referred to as the micro-necklaces along with AgBr in this paper. The elemental analysis result of as-prepared Ag(Cl,Br)-Au micro-necklaces by SEM-EDS spectrum is exhibited in **Fig. 6**. It is clear that the elements chlorine, bromine, silver and gold have all been detected, and the approximate atom concentration ratio for Cl and Br is 2:1 (**Fig. 6b**), revealing that the content of chlorine atoms became even more than bromine atoms after the immersion reaction in HAuCl₄ aqueous solution. Therefore, it is supposed that the properties of these novel Ag(Cl,Br)-Au micro-necklaces should be more similar to AgCl rather than the original AgBr template. Besides, it is also notable that the surfaces of these Ag(Cl,Br)-Au and AgBr micro-necklaces seem quite rough in high-magnification SEM images of **Fig. 6a** and **Fig. 4d**, reflecting the rationality for these micro-necklaces to have large surface areas, and further have the chance to provide large amounts of surface active sites and thereby appreciable photocatalytic performance for degradation of SDI molecules.

Fig. 7a displays the UV-vis-NIR DRS spectra of the obtained Ag(Cl,Br)-Au as well as AgBr micro-necklaces. As can be seen, the Ag(Cl,Br)-Au micro-necklaces exhibit stronger light absorption capability in visible band compared to the AgBr micro-necklaces, suggesting that these unique Ag(Cl,Br)-Au micro-necklaces could be utilized as high-performance visible-light-driven photocatalysts. Since the optical absorption properties of different silver halides including AgCl and AgBr should be quite similar to each other according to various literature reports, [66–68] the enhancement in light absorption from AgBr to Ag(Cl,Br)-Au micro-

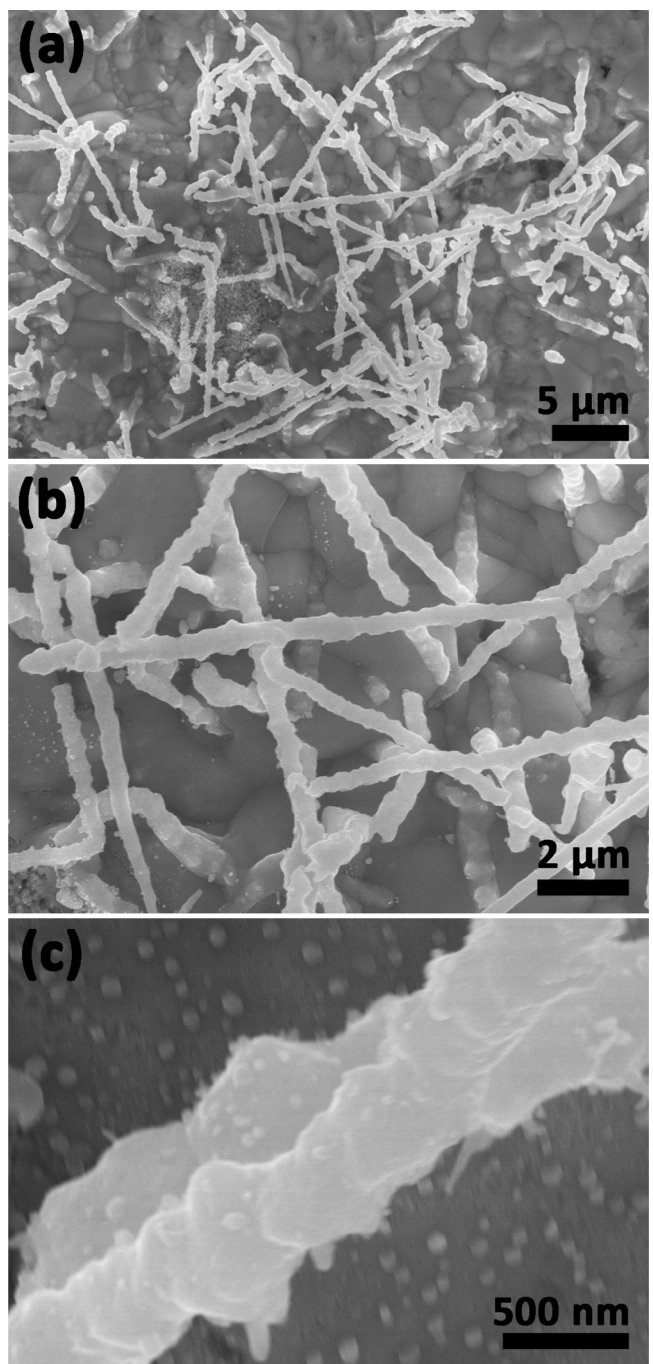


Fig. 5. Representative SEM images recorded at different magnifications of the finally obtained Ag(Cl,Br)-Au micro-necklaces.

necklaces might be ascribed mainly to the surface plasmon resonance of small gold nanoparticles decorated on the surface of these micro-necklaces. The characteristic band appeared at around 520 nm which can be distinguished from the orange curve in **Fig. 7a** (i.e. the Ag(Cl,Br)-Au micro-necklaces) matches well with the literature value of surface plasmon resonance band of gold nanoparticles. [69] The DF optical image of as-obtained Ag(Cl,Br)-Au micro-necklaces is further given in **Fig. 7b**. In addition, since the size of the gold nanoparticles decorated on Ag(Cl,Br) micro-necklaces varied mainly from several tens of nanometers to 100 nm, the DF image of the 100 nm gold colloidal nanoparticles deposited on a silicon wafer is also displayed in the insert of **Fig. 7b** as the reference. As can be seen, the colorful dots distributed

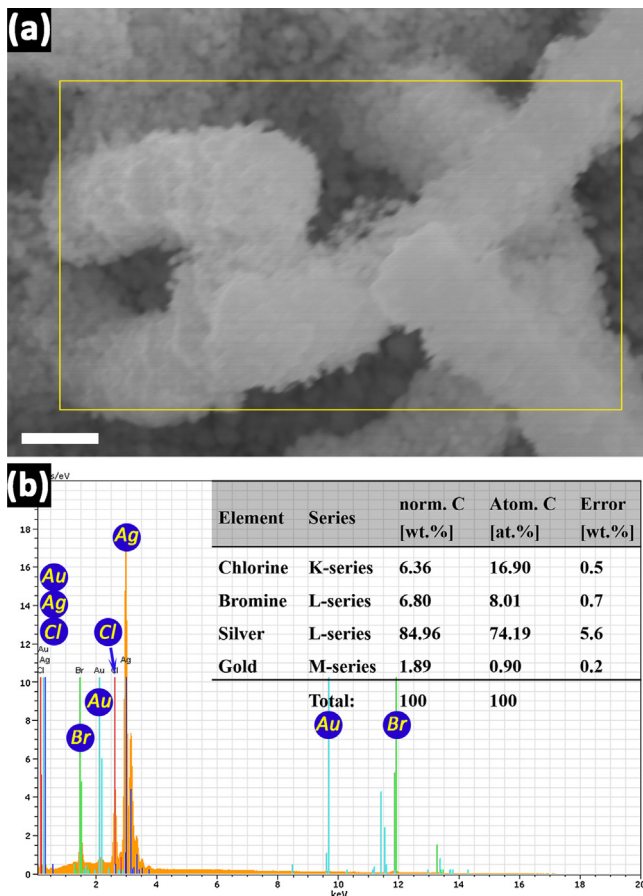


Fig. 6. SEM-EDS analysis results of the obtained Ag(Cl,Br)-Au micro-necklaces. The EDS spectrum exhibited in panel (b) was recorded from the yellow-box-marked area in panel (a). The scale bar for the SEM image in panel (a) is 500 nm.

along different lines which were originated from the optical scattering of white light by the strong surface plasmon resonance of gold nanoparticles could also be regarded as an indirect evidence for the possibility of enhancing visible light absorption properties of the micro-necklaces by the strong light confinement and multiple reflection and scattering of gold nanoparticles decorated on the surfaces [70]. Besides, because the scattering cross-sections of gold nanoparticles are generally many times their geometric size [71], it should be reasonable that the size of the scattering light spots in DF image of the gold nanoparticles is estimated to be several hundred nanometers, due to the fact that their geometric size is several tens of nanometers according to SEM images.

Owing to the designed decoration of gold nanoparticles on these micro-necklaces, distinct SERS signals of the food contaminant, SDI molecules have been detected at low concentrations on as-obtained Ag(Cl,Br)-Au micro-necklace substrates, confirming their promising potential for efficient SERS detection. Fig. 8a shows the room-temperature SERS spectra of SDI dilute solutions with different concentrations recorded on AgBr and Ag(Cl,Br)-Au micro-necklaces substrates, and further the detailed assignment for characteristic Raman scattering bands of SDI molecules is summarized in Table 1. It is obvious that when exploiting AgBr micro-necklaces as the substrate, almost no SERS signals could be observed in the spectrum at a concentration of 10^{-6} M. However, when coming to the case of Ag(Cl,Br)-Au substrates, the LOD for SDI molecules of as low as 10^{-10} M has been achieved with the characteristic Raman bands derived from the mixed modes of in-plane deformation of C–H and N–H bonds (1005 cm^{-1}), in-plane deformation of C–H bond and stretching mode of C–H bonds on phenyl/naphthyl rings (1130 cm^{-1}), in-plane deformation of C–H and N–H bonds as well as the stretching mode of C=C bonds on phenyl/naphthyl rings (1240 cm^{-1}), in-plane deformation of C–H bond and stretching mode of C–C bond (1277 , 1455 and 1560 cm^{-1}), in-plane deformation of C–H bond as well as stretching modes of C–C, C=O and N=N bonds (1392 cm^{-1}), and the in-plane deformation of C–H bond as well as stretching modes of C–C bond and C=C bond on phenyl/naphthyl rings (1589 cm^{-1}) being determined. [26,27,72] The huge enhancement of Raman signals and the subsequently low LOD came mainly from the strong light-induced

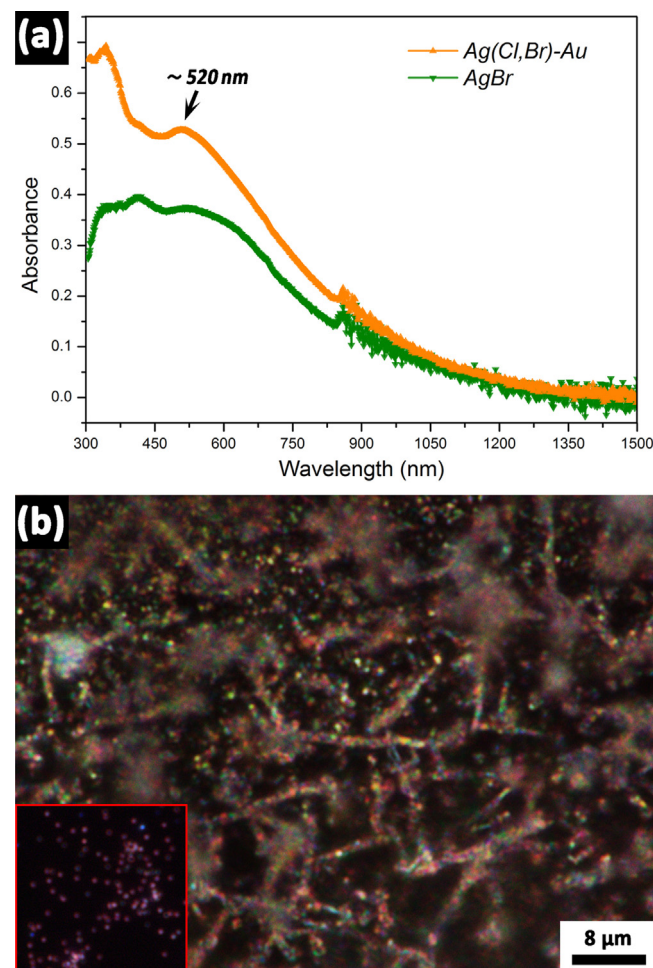


Fig. 7. (a) UV-vis-NIR diffuse reflectance spectra (DRS) of the synthesized AgBr and Ag(Cl,Br)-Au micro-necklaces grown on silver foils; (b) The dark-field (DF) optical micrograph of the obtained Ag(Cl,Br)-Au micro-necklaces. The insert gives the DF image of the purchased gold colloidal nanoparticles with the average size of about 100 nm deposited on a silicon wafer for reference.

Table 1

Room-temperature SERS spectral data and the corresponding band assignment for SDI molecules on the Ag(Cl,Br)-Au micro-necklaces substrate, where ν and δ in the table stand for the stretching mode and in-plane bending/deformation mode respectively, and Ph and Naph represent the phenyl and naphthyl functional groups respectively.

Band position (cm^{-1})	Assignment
1005	$\delta(\text{C}-\text{H}), \delta(\text{N}-\text{H})$
1130	$\delta(\text{C}-\text{H}), \nu(\text{Ph}/\text{Naph}\text{ C}-\text{H})$
1240	$\delta(\text{C}-\text{H}), \delta(\text{N}-\text{H}), \nu(\text{Ph}/\text{Naph}\text{ C}=\text{C})$
1277	$\delta(\text{C}-\text{H}), \nu(\text{C}-\text{C})$
1392	$\delta(\text{C}-\text{H}), \nu(\text{C}-\text{C}), \nu(\text{C}=\text{O}), \nu(\text{N}=\text{N})$
1455	$\delta(\text{C}-\text{H}), \nu(\text{C}-\text{C})$
1560	$\delta(\text{C}-\text{H}), \nu(\text{C}-\text{C})$
1589	$\delta(\text{C}-\text{H}), \nu(\text{C}-\text{C}), \nu(\text{Ph}/\text{Naph}\text{ C}=\text{C})$

phenyl/naphthyl rings (1130 cm^{-1}), in-plane deformation of C–H and N–H bonds as well as the stretching mode of C=C bonds on phenyl/naphthyl rings (1240 cm^{-1}), in-plane deformation of C–H bond and stretching mode of C–C bond (1277 , 1455 and 1560 cm^{-1}), in-plane deformation of C–H bond as well as stretching modes of C–C, C=O and N=N bonds (1392 cm^{-1}), and the in-plane deformation of C–H bond as well as stretching modes of C–C bond and C=C bond on phenyl/naphthyl rings (1589 cm^{-1}) being determined. [26,27,72] The huge enhancement of Raman signals and the subsequently low LOD came mainly from the strong light-induced

Table 2

A summary for the fitted pseudo-first order kinetic rate constants (k), kinetics equations, adjusted regression coefficients ($Adj.-R^2$) of the photocatalytic degradation reactions of SDI molecules, as well as the photocatalytic degradation efficiencies after 18 min of visible light (≥ 420 nm) irradiation (η_1), and the efficiency maintenance (i.e. normalized degradation efficiencies) after five cycles (normalized η_5) and twelve cycles (normalized η_{12}) of the photocatalytic degradation reaction using AgBr, AgBr–Au and Ag(Cl,Br)–Au micro-necklaces as the photocatalyst, respectively.

Photocatalyst	k (min $^{-1}$)	Kinetics equation	$Adj.-R^2$	η_1	normalized η_5	normalized η_{12}
AgBr	0.059	$y = 0.059x - 0.028$	0.997	65.1%	76.2%	2.4%
AgBr–Au	0.081	$y = 0.081x - 0.048$	0.988	80.8%	83.9%	33.6%
Ag(Cl,Br)–Au	0.180	$y = 0.180x - 0.201$	0.952	99.9%	89.6%	65.3%

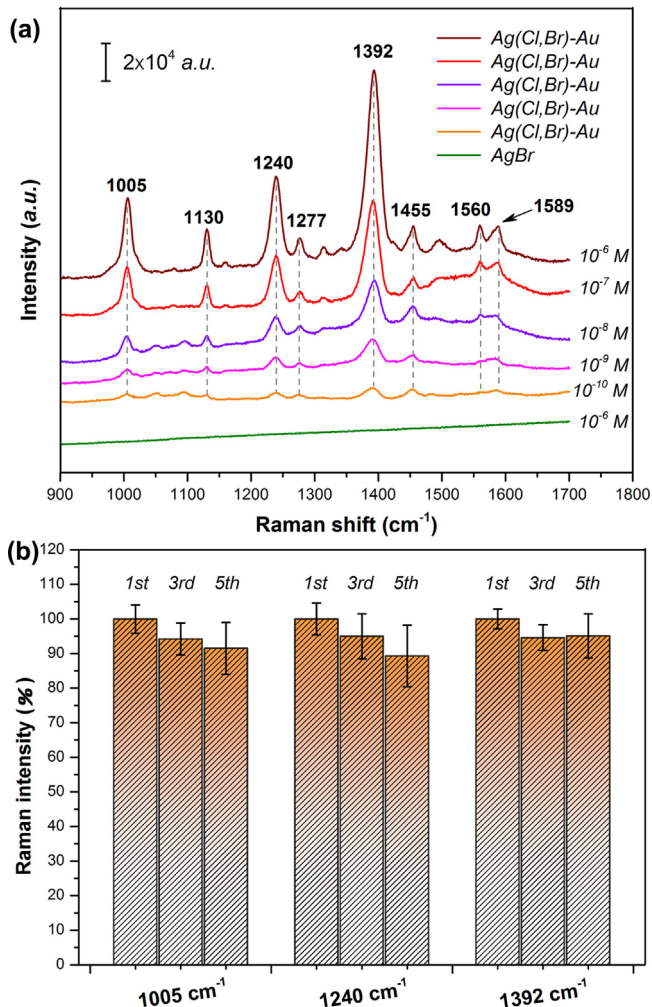


Fig. 8. (a) Room-temperature SERS spectra of the SDI dilute solutions with different concentrations collected on the AgBr and Ag(Cl,Br)-Au micro-necklaces substrates. (b) Results of the recyclability test of the prepared Ag(Cl,Br)-Au micro-necklaces substrate using the intensity maintenance of three characteristic Raman scattering bands located at 1005, 1240 and 1392 cm⁻¹ respectively after three and five cycles of SERS measurement of the 10⁻⁶ M SDI solutions as models.

electromagnetic field caused by the localized surface plasmon resonance immediately surrounding the junctions of roughened surfaces of small gold nanoparticles (i.e. the hot spots) under laser excitation. [73] In order to verify the chloride doping effect on the performance of these Ag(Cl,Br)-Au micro-necklaces, as-purchased gold nanoparticles with the average size of about 100 nm were also deposited directly on AgBr micro-necklaces, referred to as AgBr–Au, as the control sample. The deposition density was estimated by counting the number of scattering light spots in the recorded optical DF images of Ag(Cl,Br)-Au micro-necklaces, and was approximate to be 77.82 particles/ μm^2 . As shown in Fig. S3 of the Supplementary data, the SERS spectrum of 10⁻¹⁰ M SDI solution was also measured on the AgBr–Au control sample substrate. It is obvious that simi-

lar fingerprint features of SDI molecules can be observed in Fig. S3, further confirming that the SERS activity of these composite substrates generated mainly from the gold nanoparticles on the surface. The low LOD for SDI of 10⁻¹⁰ M might also have benefited from the quasi-one-dimensional shapes of the supporting Ag(Cl,Br) and AgBr micro-necklaces, owing to the possibly existed waveguide and microcavity effects according to previous studies. [74–76] Furthermore, the recyclability and stability of these Ag(Cl,Br)-Au micro-necklaces as SERS substrates have also been examined by repeating the SERS detection process under the same conditions for five cycles. As demonstrated in Fig. 8b, the SERS signals at 1005, 1240 and 1392 cm⁻¹ of Raman shift maintained intensities of 91.5%, 89.3% and 95.1% respectively after five cycles of SERS measurement of 10⁻⁶ M SDI dilute solutions, by which robust stability of Ag(Cl,Br)-Au micro-necklaces as SERS substrates could be deduced.

On the other hand, the photocatalytic performance of the obtained Ag(Cl,Br)-Au, as well as AgBr and AgBr–Au micro-necklaces for degrading SDI molecules (10⁻⁶ M) under visible light irradiation (≥ 420 nm) has been presented in Fig. 9 and Table 2. It could be known in Fig. 9a that after immersing the AgBr, AgBr–Au as well as Ag(Cl,Br)-Au micro-necklaces into SDI solutions in the dark for an hour, the solution concentrations decreased a bit maybe due to the absorption of dye molecules on the surfaces of the micro-necklaces, and when they were consequently irradiated by visible light, the concentrations of these SDI solutions decreased rapidly because of the degradation reaction catalyzed by the AgBr, AgBr–Au and Ag(Cl,Br)-Au photocatalysts, as demonstrated by Fig. 9a and the irradiation time-dependent absorption intensity in UV-vis spectra of the SDI solution shown in Fig. S4 of the Supplementary data. Particularly, it can be known from Fig. 9a and Table 2 that after 18 min of visible light irradiation, about 65.1%, 80.8% and almost 100% of the degradation efficiency for 10⁻⁶ M SDI solutions have been achieved by the AgBr, AgBr–Au and Ag(Cl,Br)-Au photocatalyst with the pseudo-first-order kinetics equations fitted to be $y = 0.059x - 0.028$, $y = 0.081x - 0.048$ and $y = 0.180x - 0.201$, respectively (insert of Fig. 9a). These micro-necklaces as photocatalysts, could generate numerous positive holes and electrons on the surface by the excitation of visible light. The reaction between positive holes and absorbed water molecules would form hydroxyl radical species. There is a series of possibilities involved in the formation of hydroxyl radical species by electron pathways. The SDI dye then degraded by attacks from either direct holes or hydroxyl species. [77] Matsui et al. have studied the degradation mechanism of SDI molecules by electrophilic oxidant O₃. [78] Since generated hydroxyl radical species in SDI solutions are similar electrophilic oxidants and have strong hydrogen abstraction ability, [79] it should be possible that the consequently formed organic radicals after attacks of SDI molecules by hydroxyl species and pristine holes would further react with oxygen molecules or other hydroxyl species to form peroxide radical species, and finally degrade through Russell mechanisms. [80–84]

The recyclability and stability of these Ag(Cl,Br)-Au as well as AgBr and AgBr–Au micro-necklaces as photocatalysts were also investigated by repeating the photocatalytic degradation reaction of SDI solutions for 12 cycles in total. As shown in Fig. 9b–c and also summarized in Table 2, the degradation efficiency for 10⁻⁶ M

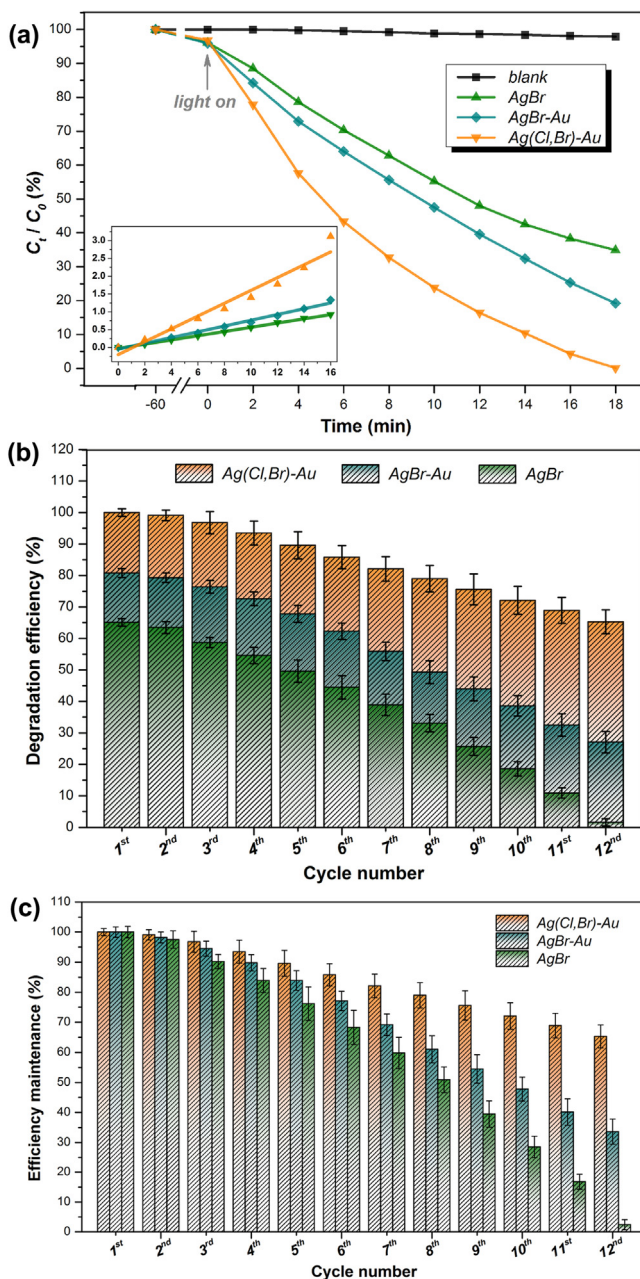


Fig. 9. Photocatalytic degradation performance of the Ag(Cl,Br)-Au micro-necklaces, as well as AgBr and AgBr-Au control samples under visible light irradiation ($\geq 420\text{ nm}$) for SDI molecules (10^{-6} M): (a) Time-dependent degradation efficiencies of SDI molecules with no catalyst and with the AgBr, AgBr-Au and Ag(Cl,Br)-Au micro-necklaces as the catalyst after immersing in the dark for 1 h. The insert demonstrates the fitted pseudo-first-order kinetic rate plots of the photocatalytic degradation reactions of SDI molecules using the AgBr, AgBr-Au and Ag(Cl,Br)-Au photocatalyst, respectively. (b) The degradation efficiencies of 10^{-6} M SDI solutions after each 18 min as one cycle of the photocatalytic reaction (12 cycles in total), and (c) the normalized degradation efficiencies (i.e. efficiency maintenance) of the Ag(Cl,Br)-Au micro-necklaces photocatalyst as well as the AgBr and AgBr-Au control samples during the 12 cycle recyclability test.

SDI solutions of AgBr decreased sharply from 65.1% of the 1st cycle to 49.6% of the 5th cycle, and finally to 1.6% of the 12th cycle. Meanwhile, the degradation efficiency achieved by AgBr-Au also decreased rapidly from 80.8% of the 1st cycle to 67.8% of the 5th cycle and 27.1% of the 12th cycle. Nonetheless, it is mentionable that in the case of Ag(Cl,Br)-Au micro-necklaces, above 65% of degradation efficiency has been maintained even after 12 cycles of the reaction. In other words, not only the absolute values of

high efficiency, but also greatly enhanced efficiency maintenance (i.e. normalized efficiency, Fig. 9c) of about 65.1% was disclosed by the Ag(Cl,Br)-Au micro-necklaces photocatalyst after 12 cycles of the degradation reaction, which was much higher than 2.4% of the AgBr and 33.6% of the AgBr-Au control samples. Additionally, the XRD pattern of Ag(Cl,Br)-Au micro-necklaces after 12 cycles of the degradation reaction, shown in Fig. S5 of the Supplementary data, further demonstrates the stability of these Ag(Cl,Br)-Au composites as the photocatalyst, since no distinct phase changes of Ag(Cl,Br)-Au can be identified before and after the 12-cycle stability test.

Overall, the superior stability and also efficiency of the Ag(Cl,Br)-Au micro-necklaces than AgBr and AgBr-Au control samples as photocatalysts could be attributed to the synergistic effect of partially substituting bromine atoms by chlorine atoms in crystalline lattices and the decoration of gold nanoparticles on the surface. For one thing, as has been discussed above, the properties of as-obtained Ag(Cl,Br) micro-necklaces should be more similar to AgCl rather than AgBr. According to previous studies, [85,86] the ionic conductivity of AgCl microcrystals ($\sim 5 \times 10^{-8} \Omega^{-1} \text{ cm}^{-1}$) with interstitial silver ions as carriers is smaller than that of AgBr ($\sim 5 \times 10^{-6} \Omega^{-1} \text{ cm}^{-1}$). Hence, the transport rate of photoelectrons from the interior to the surface of AgCl microcrystals should be larger than AgBr because the concentration of silver ions acting as temporal traps and determining the drift mobility of photoelectrons in the bulk is smaller. At the same time, the transport of photoholes from the interior to the surface of AgCl microcrystals could be smoothed as well under the condition that almost all traps should be occupied by positive holes under strong illumination for a long time. Besides, the rate of oxidation of SDI molecules by photoholes of AgCl evaluated by the height of the valence band is also higher than that of AgBr microcrystals. These three mechanisms together ensured the obtained Ag(Cl,Br) micro-necklaces of higher photocatalytic efficiency than AgBr. On the other hand, the much smaller ionic conductivity induced by interstitial silver ions in Ag(Cl,Br) micro-necklaces also led to less undesired combination between positive silver ions and photoelectrons near the surface, and thereafter inhibited the photolysis of silver halides and generation of silver clusters, resulting in promoted stability of Ag(Cl,Br) than AgBr as photocatalysts.

For another thing, the decoration of plasmonic gold nanoparticles on the surfaces of semiconductor micro-necklaces can also enhance the photocatalytic performance *via* the following two aspects [87–89]. First, the capability of plasmonic nanoparticles to confine light into small volumes at the noble metal–semiconductor interfaces together with the consequently derived hot-electron injection effect as well as plasmon resonance energy transfer to semiconductor surfaces could help to enhance the catalytic efficiency of as-prepared micro-necklaces photocatalyst. Second, regarding the stability, the decorated gold nanoparticles could reserve the photogenerated electrons as the electron sink due to their better electron affinity than semiconducting silver halides and thereby decrease the recombination rate of photogenerated electron/hole pairs, and finally contribute to the significantly enhanced stability and durability of the Ag(Cl,Br)-Au micro-necklaces than AgBr as novel visible-light-driven photocatalysts for degrading SDI molecules.

4. Conclusions

In summary, for the first time we present the novel Ag(Cl,Br)-Au micro-necklaces as efficient and stable substrate materials for both sensitive SERS detection and rapid photocatalytic degradation of food contaminant SDI molecules. On the one hand, as the photocatalyst, the Ag(Cl,Br)-Au micro-necklaces demonstrated enhanced

degradation efficiency of 10^{-6} M SDI solutions from 65.1% achieved by AgBr and 80.8% achieved by AgBr–Au to 100% after 18 min of visible light irradiation due to the synergistic effect of partial substitution of Br by Cl atoms in crystalline lattices and the decoration of Au nanoparticles on the surface. It is also mentionable that these Ag(Cl,Br)–Au micro-necklaces exhibited significantly enhanced efficiency maintenance than AgBr and AgBr–Au control samples, about 90% and 65% of after five and twelve cycles of the photocatalytic degradation reaction, which might be attributed to the low ionic conductivity induced less photolysis of silver halides and efficient charge separation promoted by Au nanoparticles on the surface. On the other hand, the designed decoration of Au nanoparticles on surfaces also endowed these micro-necklaces with considerable SERS activity for trace detection of SDI molecules with the limit of detection reaching as low as 10^{-10} M. To conclude, the novel structures, facile preparation as well as attractive application potential in both SERS detection and visible-light-driven photocatalytic degradation of SDI molecules together suggest many exciting opportunities of using these Ag(Cl,Br)–Au micro-necklaces for developing novel multifunctional devices toward environmental and health-related applications.

Acknowledgements

This work was supported by the Ministry of Science and Technology of China (973 Project No. 2013CB932901), and the National Natural Science Foundation of China (Nos. 11274066, 51172047, 51102050, U1330118). This project was sponsored by Shanghai Pujiang Program and “Shu Guang” project of Shanghai Municipal Education Commission and Shanghai Education Development Foundation (09SG01). A part of this work was supported by “Nanotechnology Platform Project” (No. 12024046) of the Ministry of Education, Culture, Sports, Science and Technology (MEXT) of Japan. Q. Cao acknowledges the support of China Scholarship Council (No. 201506100018).

Appendix A. Supplementary data

Supplementary data associated with this article can be found, in the online version, at <http://dx.doi.org/10.1016/j.apcatb.2016.09.002>, including additional discussions on reactions between AgBr and HAuCl₄ and the component of noble metal nanoparticles, HRTEM characterization results of as-obtained Ag(Cl,Br) micro-crystals and Au nanoparticles of the micro-necklaces (Fig. S1–S2), SERS spectrum of 10^{-10} M SDI solution recorded on AgBr–Au control sample substrate (Fig. S3), UV-vis absorbance spectra of the 10^{-6} M SDI solution with Ag(Cl,Br)–Au micro-necklaces as the catalyst under visible light irradiation (≥ 420 nm, Fig. S4), and the XRD pattern of the Ag(Cl,Br)–Au micro-necklaces after 12 cycles of the photocatalytic SDI degradation reaction (Fig. S5).

References

- [1] M. Stiborová, V. Martínek, H. Rýdlová, P. Hodek, E. Frei, Sudan I is a potential carcinogen for humans: evidence for its metabolic activation and detoxication by human recombinant cytochrome P450 1A1 and liver microsomes, *Cancer Res.* 62 (2002) 5678–5684.
- [2] M. Stiborová, V. Martínek, H. Rýdlová, T. Koblas, P. Hodek, Expression of cytochrome P450 1A1 and its contribution to oxidation of a potential human carcinogen 1-Phenylazo-2-Naphthol (Sudan I) in human livers, *Cancer Lett.* 220 (2005) 145–154.
- [3] Y. An, L.P. Jiang, J. Cao, C.Y. Geng, L.F. Zhong, Sudan I induces genotoxic effects and oxidative DNA damage in HepG2Cells, *Mutat. Res.* 627 (2007) 164–170.
- [4] X.L. Ye, J. Zhang, H. Chen, X.H. Wang, F. Huang, Fluorescent nanomicelles for selective detection of Sudan dye in pluronic F127 aqueous media, *ACS Appl. Mater. Interfaces* 6 (2014) 5113–5121.
- [5] L.P. Wu, Y.F. Li, C.Z. Huang, Q. Zhang, Visual detection of Sudan dyes based on the plasmon resonance light scattering signals of silver nanoparticles, *Anal. Chem.* 78 (2006) 5570–5577.
- [6] X.Y. Xu, X.G. Tian, L.G. Cai, Z.L. Xu, H.T. Lei, H. Wang, Y.M. Sun, Molecularly imprinted polymer based surface plasmon resonance sensors for detection of Sudan dyes, *Anal. Methods* 6 (2014) 3751–3757.
- [7] O. Chailapakul, W. Wonsawat, W. Siangproh, K. Grudpan, Y.F. Zhao, Z.W. Zhu, Analysis of sudan I, sudan II, sudan III, and Sudan IV in food by HPLC with electrochemical detection: comparison of glassy carbon electrode with carbon nanotube-ionic liquid gel modified electrode, *Food Chem.* 109 (2008) 876–882.
- [8] V. Cornet, Y. Govaert, G. Moens, J. Van Loco, J.M. Degroodt, Development of a fast analytical method for the determination of Sudan dyes in chili- and curry-containing foodstuffs by high-performance liquid chromatography-photodiode array detection, *J. Agric. Food Chem.* 54 (2006) 639–644.
- [9] F. Puoci, C. Garreffa, F. Iemma, R. Muzzalupo, U.G. Spizzirri, N. Picci, Molecularly imprinted solid phase extraction for detection of Sudan I in food matrices, *Food Chem.* 93 (2005) 349–353.
- [10] S. Wang, Z.X. Xu, G.Z. Fang, Z.J. Duan, Y. Zhang, S. Chen, Synthesis and characterization of a molecularly imprinted silica gel sorbent for the on-line determination of trace Sudan I in chili powder through high-performance liquid chromatography, *J. Agr. Food Chem.* 55 (2007) 3869–3876.
- [11] M. Oplatowska, P.J. Stevenson, C. Schulz, L. Hartig, C.T. Elliott, Development of a simple gel permeation clean-up procedure coupled to a rapid disequilibrium enzyme-linked immunosorbent assay (ELISA) for the detection of Sudan I dye in spices and sauces, *Anal. Bioanal. Chem.* 401 (2011) 1411–1422.
- [12] Y.Z. Wang, H. Yang, B. Wang, A.P. Deng, A sensitive and selective direct competitive enzyme-linked immunosorbent assay for fast detection of Sudan I in food samples, *J. Sci. Food Agric.* 91 (2011) 1836–1842.
- [13] Y.Z. Wang, D.P. Wei, H. Yang, Y. Yang, W.W. Xing, Y. Li, A.P. Deng, Development of a highly sensitive and specific monoclonal antibody-based enzyme-linked immunosorbent assay (ELISA) for detection of Sudan I in food samples, *Talanta* 77 (2009) 1783–1789.
- [14] C.M. Ju, Y. Tang, H.Y. Fan, J.D. Chen, Enzyme-linked immunosorbent assay (ELISA) using a specific monoclonal antibody as a new tool to detect Sudan dyes and para red, *Anal. Chim. Acta* 621 (2008) 200–206.
- [15] D. Han, M. Yu, D. Knopp, R. Niessner, M. Wu, A.P. Deng, Development of a highly sensitive and specific enzyme-linked immunosorbent assay for detection of Sudan I in food samples, *J. Agric. Food Chem.* 55 (2007) 6424–6430.
- [16] J.H. Li, H.B. Feng, J. Li, Y.L. Feng, Y.Q. Zhang, J.B. Jiang, D. Qian, Fabrication of gold nanoparticles-decorated reduced graphene oxide as a high performance electrochemical sensing platform for the detection of toxicant Sudan I, *Electrochim. Acta* 167 (2015) 226–236.
- [17] B.L. Li, J.H. Luo, H.Q. Luo, N.B. Li, A novel conducting poly(p-aminobenzene sulphonic acid)-based electrochemical sensor for sensitive determination of Sudan I and its application for detection in food stuffs, *Food Chem.* 173 (2015) 594–599.
- [18] E. Prabakaran, K. Pandian, Amperometric detection of Sudan I in red chili powder samples using Ag nanoparticles decorated graphene oxide modified glassy carbon electrode, *Food Chem.* 166 (2015) 198–205.
- [19] L.L. Yu, Y.X. Mao, Y. Gao, L.B. Qu, Sensitive and simple voltammetric detection of Sudan I by using platinum nanoparticle-modified glassy carbon electrode in food samples, *Food Anal. Methods* 7 (2014) 1179–1185.
- [20] J. Zhang, M.L. Wang, S.T. Chao, W.C. Wang, Y. He, Z.D. Chen, Electrochemical detection of Sudan I by using an expanded graphite paste electrode, *J. Electroanal. Chem.* 685 (2012) 47–52.
- [21] K.H. Chen, Z.G. Shen, J.W. Luo, X.Y. Wang, R.C. Sun, Quaternized chitosan/silver nanoparticles composite as a SERS substrate for detecting tricyclazole and Sudan I, *Appl. Surf. Sci.* 351 (2015) 466–473.
- [22] L. Pei, Y.M. Ou, W.S. Yu, Y.X. Fan, Y.Q. Huang, K.Q. Lai, Au-Ag core-shell nanospheres for surface-enhanced Raman scattering detection of Sudan I and Sudan II in chili powder, *J. Nanomater.* 2015 (2015) 430925.
- [23] C.V. Di Anibal, L.F. Marsal, M.P. Callao, I. Ruisánchez, Surface enhanced Raman spectroscopy (SERS) and multivariable analysis as a screening tool for detecting Sudan I dye in culinary spices, *Spectrochim. Acta Part A* 87 (2012) 135–141.
- [24] Q. Cao, R.C. Che, N. Chen, Facile and rapid growth of Ag₂S microrod arrays as efficient substrates for both SERS detection and photocatalytic degradation of organic dyes, *Chem. Commun.* 50 (2014) 4931–4933.
- [25] H.Y. Lin, Q. Shao, F. Hu, R.H. Que, M.W. Shao, Gold nanoparticle substrates for recyclable surface-enhanced Raman detection of rhodamine 6G and Sudan I, *Thin Solid Films* 526 (2012) 133–138.
- [26] M.Z. Si, Y.P. Kang, R.M. Liu, Surface-enhanced Raman scattering (SERS) spectra of three kinds of azo-dye molecules on silver nanoparticles prepared by electrolysis, *Appl. Surf. Sci.* 258 (2012) 5533–5537.
- [27] X. Li, H.K. Lee, I.Y. Phang, C.K. Lee, X.Y. Ling, Superhydrophobic-oleophobic Ag nanowire platform: an analyte-concentrating and quantitative aqueous and organic toxin surface-enhanced Raman scattering sensor, *Anal. Chem.* 86 (2014) 10437–10444.
- [28] P.P. Zhang, J. Gao, X.H. Sun, An ultrasensitive, uniform and large-area surface-enhanced Raman scattering substrate based on ag or Ag/Au nanoparticles decorated Si nancone arrays, *Appl. Phys. Lett.* 106 (2015) 043103.
- [29] Q. Shao, R.H. Que, M.W. Shao, L. Cheng, S.T. Lee, Copper nanoparticles grafted on a silicon wafer and their excellent surface-enhanced Raman scattering, *Adv. Funct. Mater.* 22 (2012) 2067–2070.

- [30] Q. Shao, R.H. Que, L. Cheng, M.W. Shao, Fast one-step silicon–hydrogen bond assembly of silver nanoparticles as excellent surface-enhanced Raman scattering substrates, *RSC Adv.* 2 (2012) 1762–1764.
- [31] S.M. Nie, S.R. Emory, Probing single molecules and single nanoparticles by surface-enhanced Raman scattering, *Science* 275 (1997) 1102–1106.
- [32] X.-M. Qian, S.M. Nie, Single-molecule and single-nanoparticle SERS: from fundamental mechanisms to biomedical applications, *Chem. Soc. Rev.* 37 (2008) 912–920.
- [33] H.W. Liu, L. Zhang, X.Y. Lang, Y. Yamaguchi, H. Iwasaki, Y. Inouye, Q.K. Xue, M.W. Chen, Single molecule detection from a large-scale SERS-active $\text{Au}_{79}\text{Ag}_{21}$ substrate, *Sci. Rep.* 1 (2011) 112.
- [34] X.X. Zou, R. Silva, X.X. Huang, J.F. Al-Sharab, T. Asefa, A self-cleaning porous TiO_2 -Ag core-shell nanocomposite material for surface-enhanced Raman scattering, *Chem. Commun.* 49 (2013) 382–384.
- [35] Y. Lin, C.E. Bunker, K.A.S. Fernando, J.W. Connell, Aqueously dispersed silver nanoparticle-decorated boron nitride nanosheets for reusable, thermal oxidation-resistant surface enhanced Raman spectroscopy (SERS) devices, *ACS Appl. Mater. Interfaces* 4 (2012) 1110–1117.
- [36] X.L. Li, H.L. Hu, D.H. Li, Z.X. Shen, Q.H. Xiong, S.Z. Li, H.J. Fan, Ordered array of gold semishells on TiO_2 spheres: an ultrasensitive and recyclable SERS substrate, *ACS Appl. Mater. Interfaces* 4 (2012) 2180–2185.
- [37] Q. Cao, R.C. Che, Tailoring Au–Ag–S composite microstructures in one-pot for both SERS detection and photocatalytic degradation of plasticizers DEHA and DEHP, *ACS Appl. Mater. Interfaces* 6 (2014) 7020–7027.
- [38] M. Salmistraro, A. Schwartzberg, W. Bao, L.E. Depero, A. Weber-Bargioni, S. Cabrini, I. Alessandri, Triggering and monitoring plasmon-enhanced reactions by optical nanoantennas coupled to photocatalytic beads, *Small* 9 (2013) 3301–3307.
- [39] C.Y. Wen, F. Liao, S.S. Liu, Y. Zhao, Z.H. Kang, X.L. Zhang, M.W. Shao, Bi-functional znO-RGO-Au substrate: photocatalysts for degrading pollutants and SERS substrates for real-time monitoring, *Chem. Commun.* 49 (2013) 3049–3051.
- [40] J.E. Lim, U.J. Lee, S.H. Ahn, E. Cho, H.J. Kim, J.H. Jang, H. Son, S.K. Kim, Oxygen reduction reaction on electrodeposited PtAu alloy catalysts in the presence of phosphoric acid, *Appl. Catal., B* 165 (2015) 495–502.
- [41] M. Muniz-Miranda, SERS monitoring of the catalytic reduction of 4-nitrophenol on Ag-doped titania nanoparticles, *Appl. Catal., B* 146 (2014) 147–150.
- [42] J.M. Li, J.Y. Liu, Y. Yang, D. Qin, Bifunctional Ag@Pd-Ag nanocubes for highly sensitive monitoring of catalytic reactions by surface-enhanced Raman spectroscopy, *J. Am. Chem. Soc.* 137 (2015) 7039–7042.
- [43] H. Yang, L.Q. He, Y.W. Hu, X.H. Lu, G.R. Li, B.J. Liu, B. Ren, Y.X. Tong, P.P. Fang, Quantitative detection of photothermal and photoelectrocatalytic effects induced by SPR from Au@Pt nanoparticles, *Angew. Chem. Int. Ed.* 54 (2015) 11462–11466.
- [44] K. Zhang, J.J. Zhao, J. Ji, Y.X. Li, B.H. Liu, Quantitative label-free and real-time surface-enhanced Raman scattering monitoring of reaction kinetics using self-assembled bifunctional nanoparticle arrays, *Anal. Chem.* 87 (2015) 8702–8708.
- [45] Q. Cao, K.P. Yuan, Q.H. Liu, C.Y. Liang, X. Wang, Y.-F. Cheng, Q.Q. Li, M. Wang, R.C. Che, Porous Au–Ag alloy particles inlaid AgCl membranes As versatile plasmonic catalytic interfaces with simultaneous, in situ SERS monitoring, *ACS Appl. Mater. Interfaces* 7 (2015) 18491–18500.
- [46] T. Aarthi, P. Narahari, G. Madras, Photocatalytic degradation of azure and Sudan dyes using nano TiO_2 , *J. Hazard. Mater.* 149 (2007) 725–734.
- [47] R.B. Pachwarya, R.C. Meenab, Degradation of azo dyes ponceau S, S-IV from the wastewater of textile industries in a new photocatalytic reactor with high efficiency using recently developed photocatalyst MBIRD-11, *Energy Source Part A* 33 (2011) 1651–1660.
- [48] C.M. Coates, W. Caldwell, R.S. Alberte, P.D. Barreto, J.C. Barreto, Beta-carotene protects Sudan IV from photocatalytic degradation in a micellar model system: insights into the antioxidant properties of the golden *Staphylococcus aureus*, *World J. Microb. Biot.* 23 (2007) 1305–1310.
- [49] W.B. Liu, J. Deng, Y.B. Zhao, J.S. Xu, L. Zhou, Spectral preparation analysis and photocatalytic activities of TiO_2 films codoped with iron and nitrogen, *Spectrosc. Spectr. Anal.* 29 (2009) 1394–1397.
- [50] R. Makuri, T. Yonemura, T. Yamada, M. Yamauchi, R. Ikeda, H. Kitagawa, K. Kato, M. Takata, Size-controlled stabilization of the superionic phase to room temperature in polymer-coated AgI nanoparticles, *Nat. Mater.* 8 (2009) 476–480.
- [51] H.M. Zhang, T. Tsuchiya, C.H. Liang, K. Terabe, Size-controlled AgI/Ag heteronano wires in highly ordered alumina membranes: superionic phase stabilization and conductivity, *Nano Lett.* 15 (2015) 5161–5167.
- [52] X.F. Wang, S.F. Li, Y.Q. Ma, H.G. Yu, J.G. Yu, $\text{H}_2\text{WO}_4\text{-H}_2\text{O}/\text{Ag/AgCl}$ composite nanoplates: a plasmonic Z-scheme visible-light photocatalyst, *J. Phys. Chem. C* 115 (2011) 14648–14655.
- [53] Y.X. Tang, Z.L. Jiang, G.C. Xing, A.R. Li, P.D. Kanhere, Y.Y. Zhang, T.C. Sum, S.Z. Li, X.D. Chen, Z.L. Dong, Z. Chen, Efficient Ag@AgCl cubic cage photocatalysts profit from ultrafast plasmon-induced electron transfer processes, *Adv. Funct. Mater.* 23 (2013) 2932–2940.
- [54] C. Hu, T.W. Peng, X.X. Hu, Y.L. Nie, X.F. Zhou, J.H. Qu, H. He, Plasmon-induced photodegradation of toxic pollutants with Ag-AgI/ Al_2O_3 under visible-light irradiation, *J. Am. Chem. Soc.* 132 (2010) 857–862.
- [55] J. Jiang, H. Li, L.Z. Zhang, New insight into daylight photocatalysis of AgBr@Ag: synergistic effect between semiconductor photocatalysis and plasmonic photocatalysis, *Chem. Eur. J.* 18 (2012) 6360–6369.
- [56] P. Wang, B.B. Huang, X.Y. Qin, X.Y. Zhang, Y. Dai, J.Y. Wei, M.H. Whangbo, Ag@AgCl: a highly efficient and stable photocatalyst active under visible light, *Angew. Chem. Int. Ed.* 47 (2008) 7931–7933.
- [57] L. Kong, Z. Jiang, H.H. Lai, R.J. Nicholls, T.C. Xiao, M.O. Jones, P.P. Edwards, Unusual reactivity of visible-light-responsive agBr-BiOBr heterojunction photocatalysts, *J. Catal.* 293 (2012) 116–125.
- [58] G. Begum, J. Manna, R.K. Rana, Controlled orientation in a bio-inspired assembly of Ag/AgCl/ZnO nanostructures enables enhancement in visible-light-induced photocatalytic performance, *Chem. Eur. J.* 18 (2012) 6847–6853.
- [59] L.L. Chen, D.L. Jiang, T. He, Z.D. Wu, M. Chen, In-Situ ion exchange synthesis of hierarchical AgI/BiOI microsphere photocatalyst with enhanced photocatalytic properties, *CrystEngComm* 15 (2013) 7556–7563.
- [60] P. Wang, B.B. Huang, X.Y. Zhang, X.Y. Qin, Y. Dai, Z.Y. Wang, Z.Z. Lou, Highly efficient visible light plasmonic photocatalysts Ag@Ag(Cl,Br) and Ag@AgCl-Agl, *ChemCatChem* 3 (2011) 360–364.
- [61] Y.P. Bi, J.H. Ye, Direct conversion of commercial silver foils into high aspect ratio AgBr nanowires with enhanced photocatalytic properties, *Chem. Eur. J.* 16 (2010) 10327–10331.
- [62] S.L. Joa, J.E. Pemberton, A surface enhanced Raman scattering investigation of interfacial structure at silver electrodes in electrolyte solutions of the isomers of butanol, *Langmuir* 8 (1992) 2301–2310.
- [63] J.E. Pemberton, A.J. Shen, Electrochemical and surface enhanced Raman scattering studies of bromide ion adsorption at silver electrodes in a series of normal alcohols, *Phys. Chem. Chem. Phys.* 1 (1999) 5671–5676.
- [64] S.A. Centeno1, T. Meller, N. Kennedy, M. Wypyski, The daguerreotype surface as a SERS substrate: characterization of image deterioration in plates from the 19th century studio of southworth & hawes, *J. Raman Spectrosc.* 39 (2008) 914–921.
- [65] L. Guerrini, J.V. Garcia-Ramos, C. Domingo, S. Sanchez-Cortes, Nanosensors based on viologen functionalized silver nanoparticles: few molecules surface-enhanced Raman spectroscopy detection of polycyclic aromatic hydrocarbons in interparticle hot spots, *Anal. Chem.* 81 (2009) 1418–1425.
- [66] Y.Y. Fan, W.G. Ma, D.X. Han, S.Y. Gan, X.D. Dong, L. Niu, Convenient recycling of 3D AgX/graphene aerogels (X = Br, Cl) for efficient photocatalytic degradation of water pollutants, *Adv. Mater.* 27 (2015) 3767–3773.
- [67] W.J. Ong, L.K. Putri, L.L. Tan, S.P. Chai, S.T. Yong, Heterostructured AgX/g-C₃N₄ (X = Cl and Br) nanocomposites via a sonication-assisted deposition-precipitation approach: emerging role of halide ions in the synergistic photocatalytic reduction of carbon dioxide, *Appl. Catal. B* 180 (2016) 530–543.
- [68] C. Dong, K.L. Wu, X.W. Wei, J. Wang, L. Liu, B.B. Jiang, Nitrogen-doped graphene modified AgX@Ag (X = Br, Cl) composites with improved visible light photocatalytic activity and stability, *Appl. Catal. A* 488 (2014) 11–18.
- [69] S. Eustis, M.A. El-Sayed, Why gold nanoparticles are more precious than pretty gold: noble metal surface plasmon resonance and its enhancement of the radiative and nonradiative properties of nanocrystals of different shapes, *Chem. Soc. Rev.* 35 (2006) 209–217.
- [70] X.F. Fan, W.T. Zheng, D.J. Singh, Light scattering and surface plasmons on small spherical particles, *Light: Sci. Appl.* 3 (2014) e179.
- [71] M. Hu, C. Novo, A. Funston, H.N. Wang, H. Staleva, S.L. Zou, P. Mulvaney, Y.N. Xia, G.V. Hartland, Dark-Field microscopy studies of single metal nanoparticles: understanding the factors that influence the linewidth of the localized surface plasmon resonance, *J. Mater. Chem.* 18 (2008) 1949–1960.
- [72] A.J. Kunov-Kruse, S.B. Kristensen, C. Liu, R.W. Berg, Experimental and *ab initio* DFT calculated Raman spectrum of Sudan I, a red dye, *J. Raman Spectrosc.* 42 (2011) 1470–1478.
- [73] N. Mirsaleh-Kohan, V. Iberi, P.D. Simmons Jr., N.W. Bigelow, A. Vaschillo, M.M. Rowland, M.D. Best, S.J. Pennycook, D.J. Masiello, B.S. Guiton, J.P. Camden, Single-molecule surface-enhanced Raman scattering: can STEM/EELS image electromagnetic hot spots? *J. Phys. Chem. Lett.* 3 (2012) 2303–2309.
- [74] Y. He, C.H. Fan, S.T. Lee, Silicon nanostructures for bioapplications, *Nano Today* 5 (2010) 282–295.
- [75] M.L. Zhang, X. Fan, H.W. Zhou, M.W. Shao, J.A. Zapien, N.B. Wong, S.T. Lee, A high-Efficiency surface-enhanced Raman scattering substrate based on silicon nanowires array decorated with silver nanoparticles, *J. Phys. Chem. C* 114 (2010) 1969–1975.
- [76] M.W. Shao, L. Lu, H. Wang, S. Wang, M.L. Zhang, D.-D.-D. Ma, S.T. Lee, An ultrasensitive method: surface-enhanced Raman scattering of Ag nanoparticles from β -Silver vanadate and copper, *Chem. Commun.* (2008) 2310–2312.
- [77] T. Aarthi, P. Narahari, G. Madras, Photocatalytic degradation of azure and Sudan dyes using nano TiO_2 , *J. Hazard. Mater.* 149 (2007) 721–734.
- [78] M. Matsui, K. Shibata, Y. Takase, Ozonolysis of 1-Phenylazo-2-naphthol, *Dyes Pigm.* 5 (1984) 321–328.
- [79] O. Legrini, E. Oliveros, A.M. Braun, Photochemical processes for water treatment, *Chem. Rev.* 93 (1993) 671–698.
- [80] L. Das, S. Chatterjee, D.B. Naik, S. Adhikari, Role of surfactant derived intermediates in the efficacy and mechanism for radiation chemical degradation of a hydrophobic azo dye, 1-Phenylazo-2-naphthol, *J. Hazard. Mater.* 298 (2015) 19–27.
- [81] M. Stiborová, V. Martínek, M. Semanská, P. Hodek, M. Dračinský, J. Cvačka, H.H. Schmeiser, E. Frei, Oxidation of the carcinogenic non-aminoazo dye 1-phenylazo-2-hydroxynaphthalene (Sudan I) by cytochromes P450 and peroxidases: a comparative study, *Interdiscip. Toxicol.* 2 (2009) 195–200.

- [82] G.A. Russell, Deuterium-isotope effects in the autoxidation of aralkyl hydrocarbons: mechanism of the interaction of PEroxy radicals, *J. Am. Chem. Soc.* 79 (1957) 3871–3877.
- [83] N.A. Clinton, R.A. Kenley, T.G. Traylor, Autoxidation of acetaldehyde. III. Oxygen-labeling studies, *J. Am. Chem. Soc.* 97 (1975) 3757–3762.
- [84] K. Vinodgopal, P.V. Kamat, Enhanced rates of photocatalytic degradation of an azo dye using $\text{SnO}_2/\text{TiO}_2$ coupled semiconductor thin films, *Environ. Sci. Technol.* 29 (1995) 841–845.
- [85] T. Tani, Explanation of photocatalytic water splitting by silver chloride from viewpoint of solid state physics and photographic sensitivity of silver halides, *J. Soc. Photogr. Sci. Technol. Japan* 72 (2009) 88–94.
- [86] T. Tani, Comparison in physical properties among AgCl , AgBr , and AgI grains, *J. Imaging Sci. Technol.* 51 (2007) 197–201.
- [87] M. Li, X.F. Yu, S. Liang, X.N. Peng, Z.J. Yang, Y.L. Wang, Q.Q. Wang, Synthesis of Au-CdS core-shell hetero-nanorods with efficient exciton-plasmon interactions, *Adv. Funct. Mater.* 21 (2011) 1788–1794.
- [88] S.W. Cao, Z. Yin, J. Barber, F.Y.C. Boey, S.C.J. Loo, C. Xue, Preparation of Au-BiVO₄ heterogeneous nanostructures as highly efficient visible-light photocatalysts, *ACS Appl. Mater. Interfaces* 4 (2012) 418–423.
- [89] L.W. Zhang, L.O. Herrmann, J.J. Baumberg, Size dependent plasmonic effect on BiVO₄ photoanodes for solar water splitting, *Sci. Rep.* 5 (2015) 16660.